Electric-Field Screening in Atomically Thin Layers of MoS_2: the Role of Interlayer Coupling

Andres Castellanos-Gomez, Emmanuele Cappelluti, Rafael Roldán, Nicolás Agraït, Francisco Guinea,* and Gabino Rubio-Bollinger**

Two-dimensional crystals have recently emerged as an interesting family of materials with a large variety of electronic properties ranging from superconductors to topological insulators.[1–8] Although graphene is by far the most studied two-dimensional crystal,[9] its lack of a bandgap hampers its application in semiconducting and photonic devices. A large bandgap is a requirement, for instance, to fabricate field-effect transistors with a large current on/off ratio and low power consumption. This fact has motivated the research in other 2D crystals with a large intrinsic bandgap, such as atomically thin MoS_2.[10–16] Single-layer MoS_2 transistors have shown large in-plane mobility (200–500 $cm^2\ V^{-1}\ s^{-1}$) and a high current on/off ratio (exceeding 10^8),[17] making this material of great interest for electronic devices and sensors,[17–19] possibly also in combination with graphene.[20] A deep insight into the charge distribution and on the electric-field screening by atomically thin MoS_2 layers will allow MoS_2-based transistors to be engineered towards an improved performance, and also the role of their layered structure in electric-field screening to be understood. However, no direct measurement of the electrostatic screening length in MoS_2 layers has been reported yet. Moreover, the role of the interlayer coupling in the screening (neglected for other layered materials such as few-layer graphene) is still unclear.

The aim of this work was to study electrostatic screening by single and few-layer MoS_2 sheets by means of electrostatic force microscopy in combination with non-linear Thomas–Fermi theory to interpret the experimental results. We found that a continuum model of decoupled layers, which satisfactorily reproduces the electrostatic screening for graphene and graphite, cannot account for the experimental observations. A three-dimensional model with an interlayer hopping parameter can, on the other hand, successfully account for the observed electric field screening by MoS_2 nanolayers, indicating the important role of the interlayer coupling in the screening of MoS_2.

Figure 1a shows an optical micrograph of a multilayered MoS_2 flake deposited on a Si/SiO_2 substrate. The regions showing different colors under the optical microscope

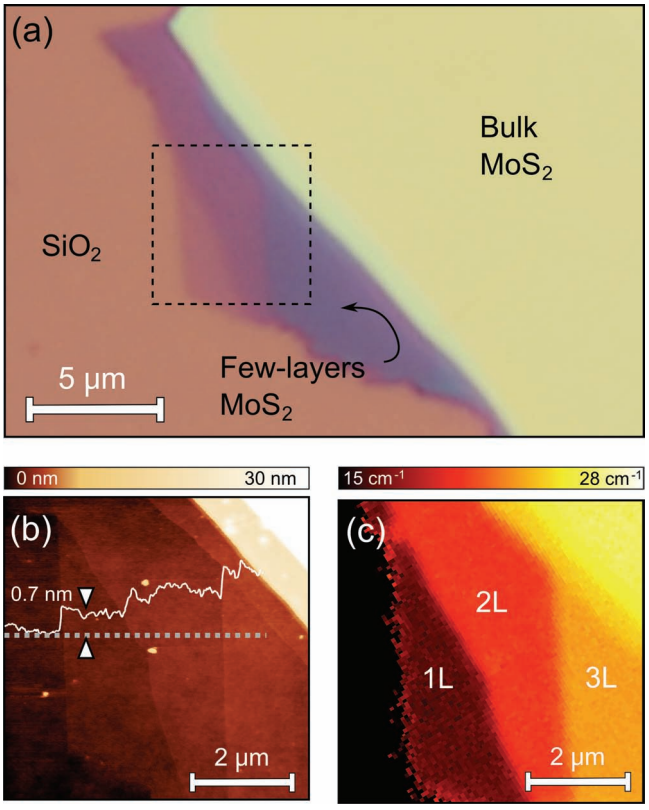

Figure 1. a) Optical micrograph of a multilayered MoS_2 flake deposited onto a 285 nm SiO_2/Si substrate. b) Topographic AFM image of the region marked by a dashed square in (a). A horizontal topographic line prolife is included in (b). c) Spatial map of the frequency difference between the E^1_{2g} and A_{1g} Raman modes, also measured in the region marked by a dashed square in (a).

Dr. A. Castellanos-Gomez
Kavli Institute of Nanoscience,
Delft University of Technology
Lorentzweg 1, 2628 CJ Delft, The Netherlands
E-mail: a.castellanosgomez@tudelft.nl
Dr. E. Cappelluti, Dr. R. Roldán, Prof. F. Guinea
Instituto de Ciencia de Materiales de Madrid, CSIC
Sor Juana Ines de la Cruz 3, 28049 Madrid, Spain
E-mail: paco.guinea@icmm.csic.es
Dr. E. Cappelluti
Institute for Complex Systems (ISC)
CNR, U.O.S. Sapienza, v. dei Taurini 19, 00185 Rome, Italy
Prof. N. Agraït
Instituto Madrileño de Estudios Avanzados en Nanociencia
IMDEA-Nanociencia
E-28049 Madrid, Spain
Prof. N. Agraït, Prof. G. Rubio-Bollinger
Departamento de Física de la Materia Condensada. Universidad Autónoma de Madrid
Campus de Cantoblanco, E-28049 Madrid, Spain
E-mail: gabino.rubio@uam.es

DOI: 10.1002/adma.201203731

correspond to zones of the flake with different numbers of layers,[21,22] with the faint purple region at the center of Figure 1a corresponding to single-layer MoS_2. Figure 1b shows an atomic force microscopy (AFM) topography image, measured in contact mode in the region marked by the dashed square in Figure 1a. A topographic line profile is also shown, indicating that the thickness of the thinner part of the flake is 0.7 nm which is compatible with the thickness of a MoS_2 single layer. Figure 1c shows a spatial map of the frequency difference between the E^1_{2g} and A_{1g} Raman modes, which increases monotonically with the number of MoS_2 layers,[23,24] measured in the area marked by the dashed rectangle in Figure 1a. The frequency-difference value clearly indicates that the number of MoS_2 layers is in good agreement with the values determined by AFM and the quantitative analysis of the optical contrast.

In order to gain a deeper insight into the interlayer screening in atomically thin MoS_2 flakes we employed electrostatic force microscopy (EFM) to probe the electric field, caused by charged impurities present at the MoS_2/substrate interface,[25,26] which is incompletely screened by the atomically thin MoS_2 crystals. The EFM measurements were carried out as follows: the AFM tip was placed 20 nm above the surface of the flake and a voltage ramp was applied to the tip while measuring the oscillation amplitude of the cantilever, which changed due to the tip-sample electrostatic force.[26] The relationship between the applied voltage and the electrostatic force is given by:[27]

$$F = \frac{1}{2}\frac{\partial C}{\partial z}\left(V_{tip} - V_s\right)^2 \quad (1)$$

where C is the tip-sample capacitance at the tip-sample distance z, V_{tip} is the tip-sample bias voltage and V_s is the surface potential of the sample. The oscillation amplitude has a parabolic dependence on the tip-sample voltage and its vertex occurs at a voltage that counteracts V_s (see **Figure 2**a). For bulk samples, the value of V_s is just the tip-sample contact potential difference (V_{CPD}) due to the work-function (Φ) difference between the tip and the sample. For atomically thin MoS_2 samples, however, the electric field generated by charged impurities at the MoS_2/substrate interface cannot be fully screened and thus V_s is modified (see sketch in Figure 2b). This effect can be seen as a shift of the parabola vertex as a function of the sample thickness, as shown in Figure 2a. We have checked that the determined V_s value does not depend on the tip-sample distance by repeating each measurement while increasing the tip-sample distance in small steps up to a total tip-sample distance of 40 nm. Additionally, we also observed that the determined value does not depend on the free-oscillation amplitude of the cantilever within the range employed in our experiment (5 nm to 2 nm).

Figure 3 shows a systematic study of the dependence of the surface potential V_s on the thickness of the MoS_2 nanosheets. While the presence of adsorbates on the surface may shift the surface potential, one can subtract this effect by considering the difference between the surface potential V_s measured in a MoS_2 nanosheet and a thick MoS_2 flake (>30 nm, considered as bulk). In this way, one thus probes directly the out-of-plane electric field screening in atomically thin MoS_2 crystals (see Figure 3a,b). For increasingly thick MoS_2 flakes, the electric field

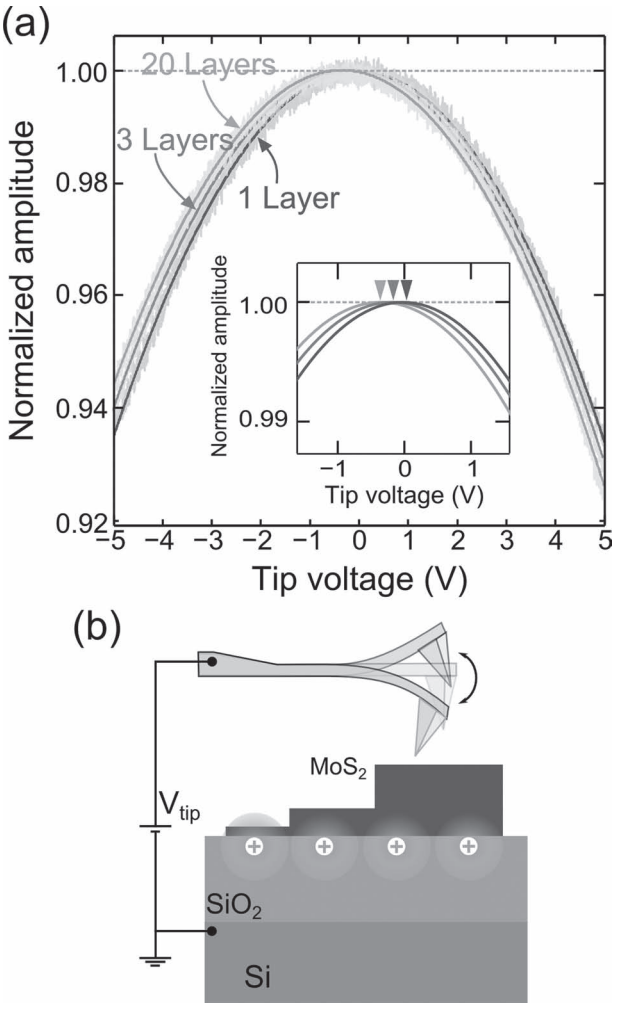

Figure 2. a) Normalized cantilever oscillation amplitude as a function of the applied tip-sample bias voltage, measured in three regions with different numbers of layers. The inset shows a magnification around the parabola maxima; only the fitting to the curves are shown to facilitate the identification of the apex (indicated by the triangles). b) Schematic of the EFM measurement setup.

generated by the charged impurities is increasingly screened, and V_s approaches the bulk value.[28,29] For small thicknesses, the sign and magnitude of the deviation from the bulk value of V_s (ΔV_s) is related to the sign and the density of the charges in the MoS_2 flakes.[29] In particular, from the decrease of ΔV_s with flake thickness, we infer negative (electron) doping, compatible with the presence of positively charged impurities in the substrate. The presence of positively charged impurities in the SiO_2 substrate is common in MoS_2-based field-effect transistor devices, showing a marked n-type behavior.[17,18,30–33]

It is interesting to notice that the dependence of $\Delta V_s(D)$ as a function of thickness is quite weak, indicating a screening as poor as that observed in graphene.[29] This appears to be quite surprising, since the poor screening in graphene is related to the linear vanishing density of states (DOS) $N(\varepsilon) \sim \varepsilon$, whereas in MoS_2 the conduction band can be described by a conventional parabolic dispersion. Dimensionality thus plays a non-trivial role here, since even a weak hopping $t_\perp$ between different layer

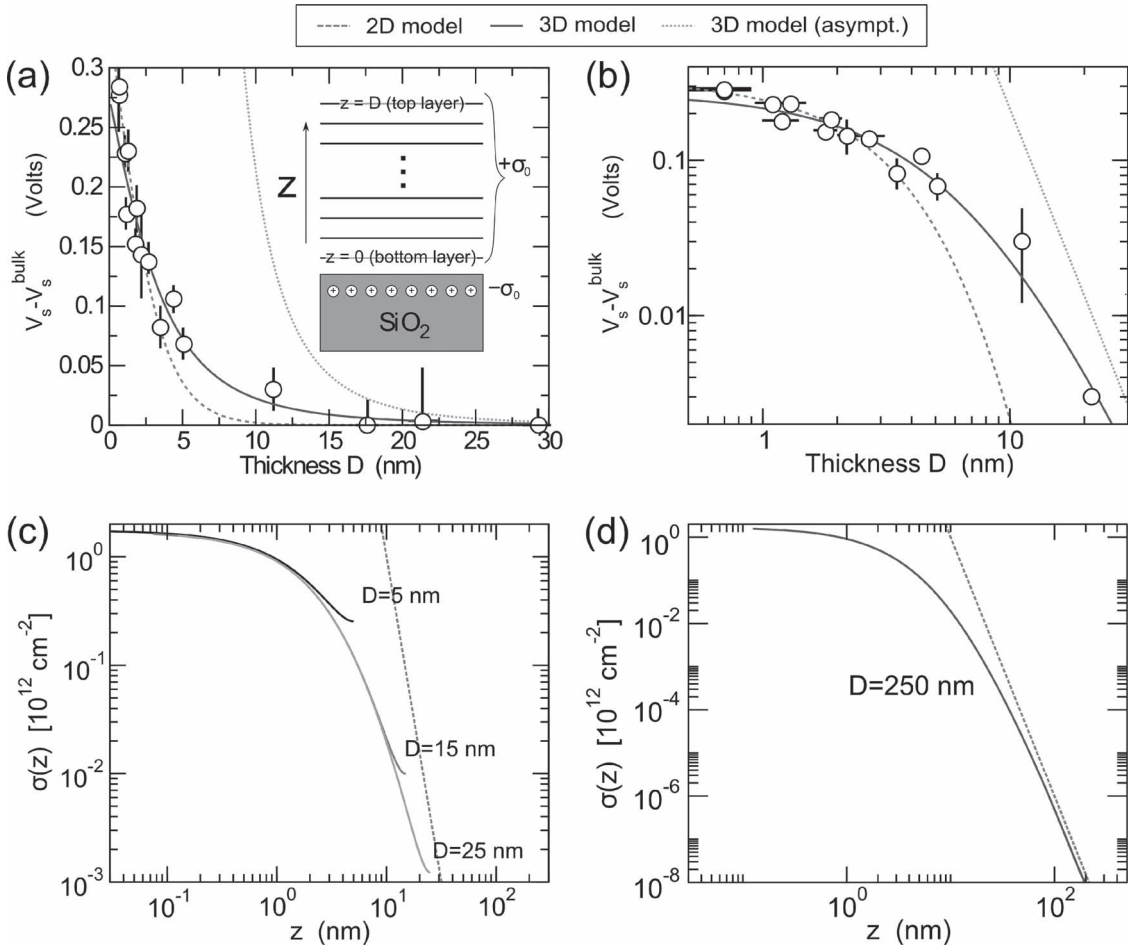

Figure 3. a) Dependence of the deviation from the bulk value of the V_s as a function of the flake thickness, caused by the electric field originated by charged impurities in the substrate, which is incompletely screened by thin flakes. The lines are the theoretical predictions for a non-linear Thomas–Fermi 2D model of uncoupled MoS_2 layers (dashed line), for the 3D model with z-axis dispersion (solid line), and for the asymptotic behavior $\Delta V_s(D) \sim 1/D^4$ of this latter one. The inset shows a sketch of the microscopic model. The vertical lines represent MoS_2 layers, while the variable $0 < z < D$ runs over the thickness of the sample. b) Same as (a) with the axes in logarithmic scale to facilitate the comparison between the experimental data and the predictions with the different models. c) Calculated surface-charge distribution, $\sigma(z)$, according to the 3D model across the samples for flakes with different thicknesses, D. The dashed line represents the strong coupling asymptotic behavior $\sigma(z) \approx z^{-6}$. d) The strong-coupling regime is reached around 100 nm.

of MoS_2 can change the low-energy DOS from $N(\varepsilon) \sim$ constant to $N(\varepsilon) \sim \varepsilon^{1/2}$.

In order to gain a quantitative insight into this issue, we employed non-linear Thomas–Fermi (TF) theory for the screening properties, as has successfully been done for graphite[34,35] and graphene.[29] Following a similar scheme to Datta et al.,[29] we first consider a continuum model of decoupled MoS_2 layers, described by a parabolic two-dimensional (2D) conduction band $\varepsilon = \hbar^2 k_{||}^2 / 2m_{||}$. As experimental values for the in-plane mass $m_{||}$ range in the literature $m_{||} \approx 0.01$–$0.1 m_e$,[36–38] the $m_{||}$ value used here was fitted (within this interval) to ensure the best agreement with the experimental data. We also take the dielectric constant along the z-axis as $\kappa_\perp = 7.4$, given in work by Molina-Sánchez and Wirtz.[39] We assume that charge transfer takes place between the MoS_2 flakes and the SiO_2 substrate, leaving a net surface charge density σ_0 and establishing an underneath layer below the substrate surface with a charge of $-\sigma_0$ (see inset in Figure 3a). The charge distribution $\sigma(z)$, as well as the electrostatic potential $V(z)$ in the multilayer samples, as functions of z (distance from the substrate) result thus from the energetic balance between the kinetic and the interlayer capacitance terms. Following Datta et al.,[29] for a sample of thickness D, we introduce a dimensionless parameter $r_D = \sigma(D)/\sigma(0)$. The screening properties are thus ruled by the implicit equation for r_D (for details see the Supporting Information):

$$\int_{r_p}^{1} \frac{du}{\left(u^2 - r_D^2\right)^{1/2}} = \sqrt{\frac{2\beta_0}{d}}\, D \Rightarrow \lim_{D\to\infty} r_D = 2\exp\left[-\sqrt{\frac{2\beta_0}{d}}\, D\right] \quad (2)$$

where $d = 6.14$ Å is the interlayer distance, and where the constant $\beta_0 = N_s N_v e^2 m_{||} / 4\pi\varepsilon_0\kappa_\perp\hbar^2$ contains all the relevant parameters of the system, like the in-plane effective mass

$m_{||}$, the interlayer dielectric constant $\kappa_{\perp}$, and the spin and valley degeneracies $N_s = N_v = 2$. Having determined r_D from the implicit solution of Equation 2, the potential drop $\Delta V(D)$ between the top and bottom layers is thus obtained as:

$$\Delta V(D) = \frac{2\pi\hbar^2\sigma_0}{N_s N_v m_{||}}\sqrt{2\beta_0 d}\,\frac{1-r_D}{\left(1-r_D^2\right)^{1/2}} \quad (3)$$

One can easily see that $\Delta V(D)$ is expected to approach its asymptotic value exponentially: $\Delta V(\infty) = \lim_{D\to\infty}\Delta V(D) = \left(2\pi\hbar^2\sigma_0 / N_s N_v m_{||}\right)\sqrt{2\beta_0 d}$.

The predictions of this model are also shown (dashed line) in Figure 3a, for $m_{||} = 0.01\ m_e$ and $\sigma_0 = 8\times10^{12}$ cm^{-2}. As we can see, this model reproduces the initial screening trend in samples a with small thickness in a satisfactory way, but it is not able to account for the long tail for large D, due to its exponential behavior. We argue that the reduced screening properties of thick flakes of multilayer MoS_2 is essentially due to the interlayer hopping, which, unlike graphene, drives multilayer MoS_2 in a "weak-coupling" regime where the characteristic screening length ξ is of the same order or larger than the sample thickness.

We can investigate this case by considering a 3D model for bulk MoS_2 with an anisotropic three-dimensional conduction band $\varepsilon = \hbar^2k_{||}^2/2m_{||} + \hbar^2k_{\perp}^2/2m_{\perp}$, where the mass $m_{||}$ is related to the interlayer hopping $t_{\perp}$ as $m_{\perp} = \hbar^2/2|t_{\perp}|d^2$. We estimate $t_{\perp} \approx -0.2$ eV from the splitting of the minimum of the conduction band as a function of the number or layers,[40] and we get, hence, $m_{||} \approx 0.5\ m_e$. Note also that in 3D bulk MoS_2 the minimum of the conduction band shifts to a finite momentum along the K-Γ direction.[41–43] so that the valley degeneracy results, $N_v = 6$.[44] Defining now $r_D = \sigma^{2/3}(D)/\sigma^{2/3}(0)$, the screening properties are determined by the implicit equation:

$$\left[\frac{25\beta_{\perp}d\sigma_0^2}{8\left(1-r_D^{5/2}\right)}\right]^{-1/10}\int_{r_D}^{1}\frac{du}{\left(u^{5/2}-r_D^{5/2}\right)^{1/2}} = \sqrt{\frac{2\beta_{\perp}}{d}}\,D \quad (4)$$

where $\beta_{\perp} = \left(4e^2/5\varepsilon_0\kappa_{\perp}\right)\left(N_s N_v d m_{||}\sqrt{m_{\perp}}/6\pi^2\hbar^3\right)^{2/3}$, and the difference potential across a sample of thickness D (see Supporting Information) is:

$$\Delta V(D) = \frac{1}{2}\left(\frac{6\pi^2\hbar^3}{N_s N_v d m_{||}\sqrt{m_{\perp}}}\right)^{2/3}\left(\frac{25\beta_{\perp}d\sigma_0^2}{8}\right)^{2/5}\frac{1-r_D}{\left(1-r_D^{5/2}\right)^{2/5}} \quad (5)$$

The potential difference $\Delta V(D)$ for such a 3D model with the same parameters as before ($m_{||} = 0.01\ m_e$, $\kappa_{\perp} = 7.4$) and a slightly smaller charge density $\sigma_0 = 5\times10^{12}$ cm^{-2} are also shown in Figure 3a (solid line), with a remarkable improvement, in particular for the long tail at large D. Note that the charge density $\sigma_0 = 5\times10^{12}$ cm^{-2} is very similar to that estimated for graphene samples on SiO_2,[25,26] suggesting that it is an intrinsic property (charged impurities) of the substrate. Note also that the reduction of the screening properties is not significantly related to the different analytical behaviors in two and three dimensions of $\Delta V(D)$ in the asymptotic strong-coupling regime, $D \to \infty$, although ΔV(D) changes from $\Delta V(D) \propto \exp(-D/\xi)$ in the 2D model to $\Delta V(D) \propto 1/D^4$ in the 3D model (dotted line in Figure 3a). The main source of the reduction of the screening properties is instead the shift towards higher D of the transition between the weak and strong coupling regimes. For instance, for the 2D model we would get such a crossover for thickness $\bar{D} \approx 1$ nm, locating thus all of the samples in the strong-coupling regime, whereas the crossover is shifted for the 3D model to $\bar{D} \approx 30$–50 nm, so that essentially most of the samples investigated here are expected to be in the weak-coupling regime, with reduced screening properties. The change of regime between weak to strong coupling is also better indicated in Figure 3c, where we report the charge density $\sigma(z)$ as function of the variable z for samples with different thickness D. We note that the strong-coupling power-law behavior $\sigma(z) \approx z^{-6}$ is asymptotically recovered only for very large $z \geq 50$ nm and for very thick samples $D \geq 100$ nm (see Figure 3d). This is quite different from the graphene case where a strong-coupling regime is achieved already for $z \geq 1$–2 nm.[29]

In conclusion, a combined experimental and theoretical study of the electrostatic screening by single and few-layer MoS_2 sheets is presented. We have probed the electric field, generated by charged impurities in the MoS_2/substrate interface, which is incompletely screened by MoS_2 sheets with different numbers of layers. A 3D non-linear Thomas–Fermi model with a non-negligible interlayer hopping parameter has been employed to reproduce the experimental results. This demonstrates that, unlike for other atomically thin crystals such as graphene, the interlayer coupling plays an important role in the screening processes for MoS_2.

Experimental Section

MoS_2 nanosheets were fabricated by mechanical exfoliation of MoS_2 (SPI Supplies, 429ML-AB) with Nitto Denko tape. In order to ensure the optical visibility of the ultrathin MoS_2 layers, Si/SiO_2 wafers with a 285 nm SiO_2 layer were used.[21] We identified single and few-layer MoS_2 sheets under an optical microscope and estimated the number of layers by their optical contrast.[21] Prior to the transfer, the Si/SiO_2 substrates were cleaned following standard procedures in nanofabrication. Firstly, the Si/SiO_2 substrate was cleaned with nitric acid in an ultrasonic bath for 5 min. Secondly, the substrates were thoroughly rinsed with deionized water. Thirdly, the substrates were immersed in isopropyl alcohol and were dried by blowing with nitrogen gas. In order to remove any organic residue from the surface, the substrates were further cleaned in a UV/Ozone generator (Novascan) for 10 min just before the transfer.

The topography of the MoS_2 nanolayers was characterized using a Nanotec Cervantes AFM. Standard silicon cantilevers with a spring constant of 40 N m^{-1} and a tip curvature <10 nm were used to operate in amplitude-modulation mode (for the EFM measurements). Softer cantilevers with a spring constant of 0.7 N m^{-1} and a tip curvature <20 nm were used to operate in contact-mode AFM. Contact-mode AFM was used to avoid thickness-determination artifacts due to the thickness-dependent surface potential of the MoS_2 flakes. The AFM piezoelectric positioners were calibrated by means of a recently developed method to provide accurate measurements of the flake thicknesses.[45]

A micro-Raman spectrometer (Renishaw in-via RM 2000) was used in a backscattering configuration excited with visible laser light (λ = 514 nm), at low power levels $P < 1$ mW to double check the number of layers of the studied MoS_2 flakes.[23,43]

COMMUNICATION

Supporting Information

Supporting Information is available from the Wiley Online Library or from the author.

Acknowledgements

This work was supported by MICINN/MINECO (Spain) through the programs MAT2011-25046 and CONSOLIDER-INGENIO-2010 "Nanociencia Molecular" CSD-2007-00010, Comunidad de Madrid through program Nanobiomagnet S2009/MAT-1726 and the European Union (FP7) through the programs RODIN and ELFOS. E.C. acknowledges a Marie Curie Grant, PIEF-GA-2009-251904.

Received: September 7, 2012
Published online: November 1, 2012

[1] K. S. Novoselov, A. K. Geim, S. V. Morozov, D. Jiang, Y. Zhang, S. V. Dubonos, I. V. Grigorieva, A. A. Firsov, *Science* **2004**, *306*, 666.
[2] C. Dean, A. Young, I. Meric, C. Lee, L. Wang, S. Sorgenfrei, K. Watanabe, T. Taniguchi, P. Kim, K. Shepard, *Nat. Nanotechnol.* **2010**, *5*, 722.
[3] H. Steinberg, D. R. Gardner, Y. S. Lee, P. Jarillo-Herrero, *Nano Lett.* **2010**, *10*, 5032.
[4] A. Castellanos-Gomez, M. Wojtaszek, N. Tombros, N. Agraït, B. J. van Wees, G. Rubio-Bollinger, *Small* **2011**, *7*, 2491.
[5] A. Castellanos-Gomez, M. Poot, A. Amor-Amorós, G. Steele, H. van der Zant, N. Agraït, G. Rubio-Bollinger, *Nano Res.* **2012**, *5*, 550.
[6] D. Teweldebrhan, V. Goyal, A. A. Balandin, *Nano Lett.* **2010**, *10*, 1209.
[7] D. Teweldebrhan, V. Goyal, M. Rahman, A. A. Balandin, *Appl. Phys. Lett.* **2010**, *96*, 053107.
[8] J. Khan, C. Nolen, D. Teweldebrhan, D. Wickramaratne, R. Lake, A. Balandin, *Appl. Phys. Lett.* **2012**, *100*, 043109.
[9] K. S. Novoselov, D. Jiang, F. Schedin, T. J. Booth, V. V. Khotkevich, S. V. Morozov, A. K. Geim, *Proc. Natl. Acad. Sci. USA* **2005**, *102*, 10451.
[10] A. Ayari, E. Cobas, O. Ogundadegbe, M. S. Fuhrer, *J. Appl. Phys.* **2007**, *101*, 014507.
[11] A. Castellanos-Gomez, M. Poot, G. A. Steele, H. S. J. van der Zant, N. Agraït, G. Rubio-Bollinger, *Adv. Mater.* **2012**, *24*, 772.
[12] A. Castellanos-Gomez, M. Poot, G. Steele, H. van der Zant, N. Agrait, G. Rubio-Bollinger, *Nanoscale Res. Lett.* **2012**, *7*, 233.
[13] K. F. Mak, K. He, J. Shan, T. F. Heinz, *Nat. Nanotechnol.* **2012**, *7*, 494.
[14] T. Cao, G. Wang, W. Han, H. Ye, C. Zhu, J. Shi, Q. Niu, P. Tan, E. Wang, B. Liu, *Nat. Commun.* **2012**, *3*, 887.
[15] S. Kim, A. Konar, W. S. Hwang, J. H. Lee, J. Lee, J. Yang, C. Jung, H. Kim, J. B. Yoo, J. Y. Choi, *Nat. Commun.* **2012**, *3*, 1011.
[16] H. Wang, L. Yu, Y.-H. Lee, Y. Shi, A. Hsu, M. L. Chin, L.-J. Li, M. Dubey, J. Kong, T. Palacios, *Nano Lett.* **2012**, *12*, 4674.
[17] B. Radisavljevic, A. Radenovic, J. Brivio, V. Giacometti, A. Kis, *Nat. Nanotechnol.* **2011**, *6*, 147.
[18] H. Li, Z. Yin, Q. He, H. Li, X. Huang, G. Lu, D. W. H. Fam, A. I. Y. Tok, Q. Zhang, H. Zhang, *Small* **2012**, *8*, 63.
[19] K. F. Mak, K. He, J. Shan, T. F. Heinz, *Nat. Nanotechnol.* **2012**, *7*, 494.
[20] L. Britnell, R. Gorbachev, R. Jalil, B. Belle, F. Schedin, A. Mishchenko, T. Georgiou, M. Katsnelson, L. Eaves, S. Morozov, *Science* **2012**, *335*, 947.
[21] A. Castellanos-Gomez, N. Agrait, G. Rubio-Bollinger, *Appl. Phys. Lett.* **2010**, *96*, 213116.
[22] H. Li, G. Lu, Z. Yin, Q. He, Q. Zhang, H. Zhang, *Small* **2012**, *8*, 682.
[23] C. Lee, H. Yan, L. E. Brus, T. F. Heinz, J. Hone, S. Ryu, *ACS Nano* **2010**, *4*, 2695.
[24] H. Li, Q. Zhang, C. C. R. Yap, B. K. Tay, T. H. T. Edwin, A. Olivier, D. Baillargeat, *Adv. Funct. Mater.* **2012**, *22*, 1385.
[25] Y. Zhang, V. W. Brar, C. Girit, A. Zettl, M. F. Crommie, *Nat. Phys.* **2009**, *5*, 722.
[26] A. Castellanos-Gomez, R. H. M. Smit, N. Agraït, G. Rubio-Bollinger, *Carbon* **2012**, *50*, 932.
[27] T. Glatzel, S. Sadewasser, M. Lux-Steiner, *Appl. Surf. Sci.* **2003**, *210*, 84.
[28] N. J. Lee, J. W. Yoo, Y. J. Choi, C. J. Kang, D. Y. Jeon, D. C. Kim, S. Seo, H. J. Chung, *Appl. Phys. Lett.* **2009**, *95*, 222107.
[29] S. S. Datta, D. R. Strachan, E. J. Mele, A. T. C. Johnson, *Nano Lett.* **2009**, *9*, 7.
[30] S. Ghatak, A. N. Pal, A. Ghosh, *ACS Nano* **2011**, *5*, 7707.
[31] Z. Yin, H. Li, L. Jiang, Y. Shi, Y. Sun, G. Lu, Q. Zhang, X. Chen, H. Zhang, *ACS Nano* **2012**, *6*, 74.
[32] A. Castellanos-Gomez, M. Barkelid, A. M. Goossens, V. E. Calado, H. S. J. van der Zant, G. A. Steele, *Nano Lett.* **2012**, *12*, 3187.
[33] W. Choi, M. Y. Cho, A. Konar, J. H. Lee, G. B. Cha, S. C. Hong, S. Kim, J. Kim, D. Jena, J. Joo, *Adv. Mater.* **2012**.
[34] S. Safran, D. Hamann, *Phys. Rev. B* **1981**, *23*, 565.
[35] L. Pietronero, S. Strässler, H. Zeller, M. Rice, *Phys. Rev. Lett.* **1978**, *41*, 763.
[36] B. Evans, P. Young, *Proc. Phys. Soc.* **1967**, *91*, 475.
[37] A. Baldereschi, M. G. Diaz, *Il Nuovo Cimento B (1965–1970)* **1970**, *68*, 217.
[38] P. Harper, *J. Phys. C: Solid State Phys.* **1974**, *7*, 1247.
[39] A. Molina-Sánchez, L. Wirtz, *Phys. Rev. B* **2011**, *84*, 155413.
[40] A. Splendiani, L. Sun, Y. Zhang, T. Li, J. Kim, C. Y. Chim, G. Galli, F. Wang, *Nano Lett.* **2010**, *10*, 1271.
[41] L. Mattheiss, *Phys. Rev. B* **1973**, *8*, 3719.
[42] S. Lebègue, O. Eriksson, *Phys. Rev. B* **2009**, *79*, 115409.
[43] K. F. Mak, C. Lee, J. Hone, J. Shan, T. F. Heinz, *Phys. Rev. Lett.* **2010**, *105*, 136805.
[44] K. Kaasbjerg, K. S. Thygesen, K. W. Jacobsen, *Phys. Rev. B* **2012**, *85*, 115317.
[45] A. Castellanos-Gomez, C. R. Arroyo, N. Agraït, G. Rubio-Bollinger, *Microsc. Microanal.* **2012**, *18*, 353.